Pergamon

Int. J. Solids Structures Vol. 34, No. 18, pp. 2321–2338, 1997

0020-7683/97 $17.00 + .00

PII: S0020-7683(96)00129-1

CONTINUOUS VS DISCONTINUOUS BRIDGED-CRACK MODEL FOR FIBER-REINFORCED MATERIALS IN FLEXURE

A. CARPINTERI
Politecnico di Torino, Department of Structural Engineering, Corso Duca degli Abruzzi, 24, 10129 Torino, Italy

and

R. MASSABÓ
Universitá di Genova, Istituto di Scienza delle Costruzioni, Via Montallegro 1, 16145 Genova, Italy

(*Received* 4 *May* 1995; *in revised form* 24 *June* 1996)

Abstract—Two different nonlinear fracture mechanics models are proposed for analysis of the constitutive flexural behavior of brittle-matrix composites with localized or distributed continuous ductile reinforcements. The models analyze the potential crises for brittle crack propagation and reinforcement yielding or debonding and can be fitted into the general framework of the bridged-crack model. A rigid-plastic bridging law is assumed. Local discontinuous phenomena, as well as a ductile to brittle transition in the constitutive relationship, when a characteristic dimension of the body decreases, are predicted. A comparison between the continuous and discontinuous formulations shows that, in the limit case of a sufficiently high number of localized reinforcements, the theoretical models converge to the same global results. © 1997 Elsevier Science Ltd.

1. INTRODUCTION

Crack growth in a brittle-matrix composite material is a discontinuous phenomenon, characterized by sudden initiations and arrests of propagation, caused by the bridging action of the secondary phases, as well as by the rise and coalescence of microcracks in the process or bridging zone. Often this local phenomenon, which is evident at a microscale level, does not translate into global discontinuous effects and the macrostructural behavior of the composite members proves globally continuous. Nevertheless, in brittle-matrix composite materials with high strength and high bond-resistance fibers, or in composites with a limited number of localized reinforcements, some discontinuous effects may emerge even at the macroscale level.

Local discontinuities, which are an indication of snap-back or snap-through instabilities for deflection-control and load-control, respectively, have been noticed in the experimental flexural response of different kinds of composites. The load-deflection diagram shown in Figure 1(a) refers to a four-point bending test on a cement beam reinforced with two localized layers of glass-fiber bundles (span × depth × thickness = 90 × 9 × 20 mm) (Zhu and Bartos, 1993). The diagram reveals snap-back instabilities, or loading jumps at constant displacement, caused by a catastrophic crack propagation arrested by the bridging action of the reinforcements. In the load-deflection diagram of Figure 1(b), resulting from a three-point bending test on a high-resistance reinforced concrete, a local snap-through instability clearly highlights the bridging action of the steel bar (span × depth × thickness = 1200 × 200 × 150 mm) (Bosco *et al.*, 1990). Finally, in Figure 1(c) a load vs deflection curve resulting from a four-point bending test on a SiC whisker-reinforced alumina is shown (span × depth × thickness = 41 × 2.5 × 2.5 mm) (Jenkins *et al.*, 1987). The curve presents a typical saw-tooth appearance which is the macrostructural result of the local discontinuous phenomena linked to successive crack propagation and arrest.

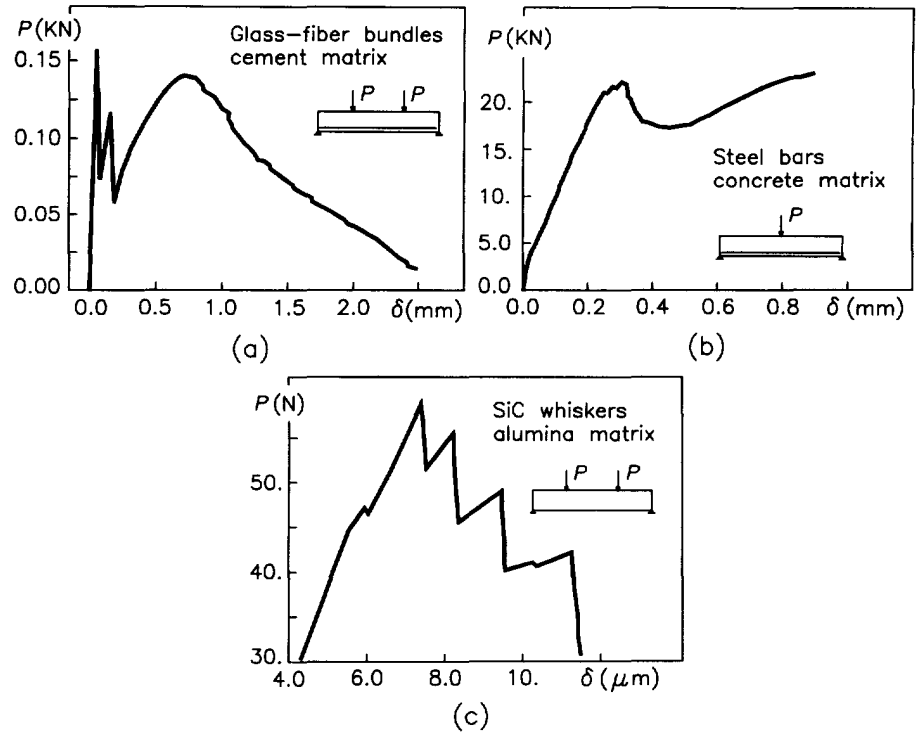

Fig. 1. Discontinuous flexural responses in various composites, after Zhu and Bartos (1993), Bosco *et al.* (1990) and Jenkins *et al.* (1987).

With the aim of analyzing the constitutive flexural response of different kinds of composite materials and of reproducing nonlinear phenomena, such as the ones previously discussed, two nonlinear fracture mechanics applications are proposed. Both the applications examine the evolutive process of crack propagation in a composite cross-section under monotonic bending and can be fitted into the general framework of the bridged-crack model.

The bridged-crack model is a nonlinear fracture mechanics model which simulates the bridging zone and the bridging mechanisms of the material through a fictitious crack and a continuous or discontinuous distribution of closing tractions, directly applied onto the crack faces. It assumes a singular stress field in the crack tip vicinity, and the crack propagates as soon as the crack tip stress intensity factor reaches the matrix toughness. Different versions of this model have been formulated for the analysis of composites with uniformly distributed reinforcements (Marshall *et al.*, 1985; Jenq and Shah, 1985; Foote *et al.*, 1986; Budiansky *et al.*, 1986; Jenq and Shah, 1986; Rose, 1987; Swanson *et al.*, 1987; Erdogan and Joseph, 1989; Cox and Marshall, 1991; Kendall *et al.*, 1991; Cox, 1991; Ballarini and Muju, 1993; Cox and Marshall, 1994). Moreover, bridged-crack models have been proposed for the analysis of the overall behavior of brittle-matrix composites with localized reinforcements, such as bars, wires, and riveted or bonded stiffeners (Romualdi and Batson, 1963; Carpinteri, 1984; Desayi and Ganesan, 1986; Bosco and Carpinteri, 1992a, b; Carpinteri and Massabó, 1994; Bosco and Carpinteri, 1995).

The *discontinuous model* proposed in this paper, replaces the secondary-phase bridging action by means of concentrated forces directly applied onto the crack faces. In this way either localized reinforcements, such as bars, bundles of fibers or wires, can be represented in a global macrostructural analysis of a composite member in bending, or microstructural modeling of a generic fiber-reinforced composite can be developed. The analysis derives from a model, originally proposed by Carpinteri (1984), for the study of the fracturing process in reinforced concrete beams. On the other hand, in the *continuous model* described in this paper, the secondary-phase restraining of crack propagation is represented by a continuous closing traction distribution acting along the crack faces. The secondary-phase

bridging action is therefore rendered homogeneous and the model can be consistently applied to analyze the failure process in brittle-matrix composites with uniformly distributed reinforcements.

The analytical formulations of the model are shown and the theoretical results are discussed and compared. The effects of the local damage process on the macrostructural behavior are investigated in the case of a bridging mechanism characterized by a rigid-plastic bridging law, linking the closing traction to the crack opening displacement. The structural behavior proves to be controlled by one dimensionless parameter, which depends on the beam depth, the matrix toughness, the fiber ultimate strength and the fiber volume ratio.

2. MODEL ASSUMPTIONS AND DIMENSIONAL ANALYSIS

The proposed theoretical models explain and reproduce the monotonic constitutive flexural response of multiphase materials. Brittle-matrix composites reinforced with continuous ductile elements, e.g. bars, wires, or fibers with a high aspect-ratio, are considered.

The models refer to the schemes shown in Figs 2(a) and 3, representing the cracked cross section of a composite beam in bending. The depth and thickness of the cross section are h and b, respectively, and the crack length is a. The normalized crack depth $\xi = a/h$ and the normalized coordinate $\zeta = x/h$ are defined, x being the generic coordinate related to the bottom of the cross section.

The continuous and discontinuous closing traction distributions, directly applied onto the crack faces in the theoretical schemes, represent the physical bridging mechanisms of

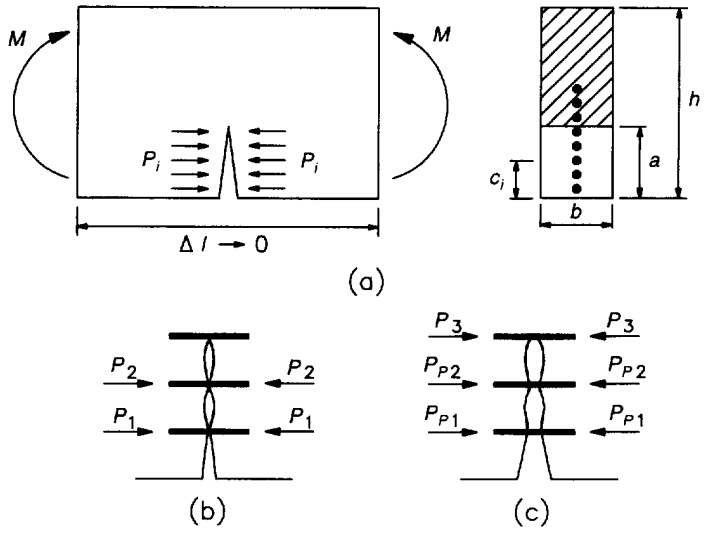

Fig. 2. (a) Schematic of the *discontinuous-model*; (b) and (c) crack profiles for elastic and yielded reinforcements.

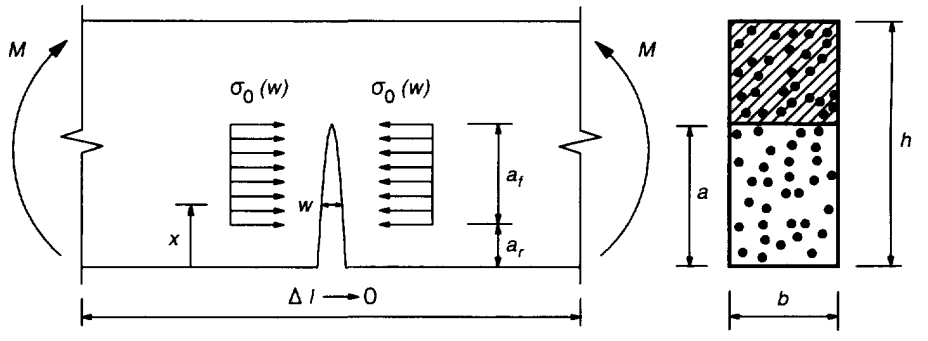

Fig. 3. Schematic of the *continuous-model*.

the reinforcing phases. In the discontinuous model (Fig. 2(a)) the indeterminate closing forces P_i $(i = 1, \ldots, m)$, replace the bridging actions of a discrete number of localized reinforcements. The coordinate of the ith reinforcement from the bottom of the beam is c_i, and the normalized value is $\zeta_i = c_i/h$. In the continuous model (Fig. 3), the closing tractions σ_0 represent the bridging action of a continuous distribution of secondary reinforcing phases.

A linear-elastic constitutive law together with a linear elastic fracture mechanics (LEFM) crack propagation condition is assumed for the matrix. The crack starts propagating when the global crack tip stress intensity factor K_I, which is a measure of the singular stress field in the crack tip vicinity, reaches the matrix toughness K_{IC}. Reference is made to the two-dimensional single-edge notched-strip solutions (Tada *et al.*, 1985) to define the fracture mechanics parameters.

The stress-strain constitutive law of the reinforcements is assumed elastic-perfectly plastic. Moreover a rigid-plastic bond-slip law is defined on account of local debonding between the matrix and the reinforcement. This law is a simplified model which is physically realistic for small slips. The last two assumptions imply a rigid-perfectly plastic bridging relationship, linking the closing tractions to the crack face openings, for the description of the secondary-phase restraining of crack propagation. In particular, in the discontinuous model the bridging relationship $P_i(w_i)$ relates the bridging force P_i to the crack opening displacement w_i at the ith fiber level, and in the continuous model the bridging relationship $\sigma_0(w)$ relates the bridging tractions σ_0 to the crack opening displacement $w(x)$, at the generic coordinate x. The maximum bridging traction is defined, in the discontinuous and in the continuous model, respectively, by the ultimate force $P_{Pi} = A_i\sigma_y$, and by the ultimate stress $\sigma_{0P} = \rho\sigma_y$, A_i being the single reinforcement area, ρ the secondary-phase volume ratio and σ_y the minimum between the reinforcement stresses at the yielding and sliding limit. Low reinforcement volume ratios are considered so that only the matrix properties control the composite elastic behavior. The composite orthotropy could be introduced in an approximate way through the evaluation of an orthotropic Young's modulus (Cox and Marshall, 1991).

The potential collapse mechanisms, due to brittle crack propagation and to yielding or sliding of the reinforcements are examined. The cross-sectional mechanical response, through the constitutive flexural relationship linking the bending moment M to the localized rotation ϕ, is then evaluated by means of the above elementary events. The potential crises are controlled by two parameters with different physical dimensions, the ultimate stress σ_y $[F][L]^{-2}$ and the critical stress intensity factor K_{IC} $[F][L]^{-1.5}$. These different dimensions make the structural behavior dependent on the beam size.

Dimensional analysis allows us to define the dimensionless parameters which synthetically control the kind of response and final collapse of the cross section (Buckingham, 1915). In accordance with the model assumptions, the functional relationship M vs ϕ may be put into the following general form:

$$\mathcal{F}(M, \phi, K_{IC}, E, \rho\sigma_y, h; r_i) = 0 \tag{1}$$

in which all the pertinent variables involved in the physical problem are considered. E is the matrix Young's modulus, and r_i are the dimensionless ratios describing the geometry of the member, e.g. the normalized thickness b/h, the normalized initial crack length a_0/h and, in the discontinuous model, the normalized reinforcement coordinates c_i/h and the single reinforcement percentage $\rho_i = A_i/bh$. The Poisson ratio is considered as negligible.

If we fix the geometrical ratios and assume the localized reinforcements of the discontinuous model as having constant area ($\rho_i = \rho/n$, n = total number of reinforcements), the choice of the dimensionally independent quantities K_{IC} and h as fundamental set, leads to the dimensionless physical equation:

$$f\left(\frac{M}{K_{IC}h^{2.5}}, \phi, \frac{\rho\sigma_y h^{0.5}}{K_{IC}}, \frac{Eh^{0.5}}{K_{IC}}\right) = f(\tilde{M}, \phi, N_P, \tilde{E}) = 0 \tag{2}$$

in which $\tilde{M}$, $\tilde{E}$ and N_P represent, respectively, the dimensionless values of the applied

moment, of Young's modulus and of the reinforcement ultimate strength. The theoretical formulation will show that the parameter $\tilde{E}$ is a simply constant divisor of the localized rotations, (see eqns (12) and (19)), so that eqn (2) becomes:

$$f(\tilde{M}, \phi, N_P) = 0 \tag{3}$$

$$N_P = \rho \frac{\sigma_y h^{0.5}}{K_{IC}} \tag{4}$$

in which the dimensionless variable N_P, controlling the brittleness of the cross section, has been called brittleness number (Carpinteri, 1981 and 1984). Equation (3) states that the structural responses are physically similar if the dimensionless number N_P remains unchanged, and therefore physical non-similarity is predicted when the size-scale of the body varies.

It is worth noting that the physical eqn (3) holds only within the range of validity of the model assumptions. We assumed a perfectly plastic law to describe the reinforcement bridging mechanism. On the other hand, if the bridging tractions vanish for crack opening displacements greater than a critical value w_c, a new governing parameter $\tilde{w}_c = w_c/h$ is expected to be involved in the functional relationship (2). According to the theoretical analysis proposed by Carpinteri and Massabó (1995), the final equation can be given the form:

$$f(\tilde{M}, \phi, N_P, \tilde{E}\tilde{w}_c) = 0. \tag{5}$$

The cross-sectional global response turns out to be governed by two dimensionless parameters, namely, N_P and the product between the dimensionless Young's modulus and the normalized critical crack opening displacement, $\tilde{E}\tilde{w}_c = (Ew_c)/(K_{IC}h^{0.5})$. The parameter $\tilde{E}\tilde{w}_c$ affects the length of the bridged crack, which can vary during the loading process because of the failure of the reinforcements. In the same way, two dimensionless parameters control the behavior of materials characterized by different bridging laws, e.g. brittle-matrix composites reinforced with short fibers or particles.

3. THE DISCONTINUOUS MODEL

Let us consider the cracked composite beam in bending shown in Fig. 2(a). The theoretical model reproduces a loading process, which is controlled by the monotonically increasing crack depth a, when the successive cross-sectional configurations that satisfy equilibrium and compatibility are evaluated. These solutions are found through the application of m proper kinematic conditions, related to the crack opening displacement w_i at the different fiber levels, which make it possible to evaluate the unknown reactions P_i and therefore to solve the statically indeterminate problem. The analytical formulation has been proposed by Bosco and Carpinteri (1995). The fundamental passages are briefly recalled as they constitute the theoretical framework upon which the continuous model of the next section is based. Moreover a direct comparison between the analytical equations of the two models can explain their differences and peculiarities.

The crack opening displacement w_i at the ith level can be defined through the superposition principle and the localized compliances due to the crack:

$$w_i = w_{iM} + \sum_{j=1}^{m} w_{ij} = \lambda_{iM} M - \sum_{j=1}^{m} \lambda_{ij} P_j \tag{6}$$

where w_{iM} and w_{ij} are the crack opening displacements produced by the bending moment M and by the generic reactions P_j, respectively; λ_{iM} and λ_{ij} are the localized compliances due to the crack, representing, respectively, the crack opening displacement due to a unit bending moment $M = 1$ and to unit opening forces $P_j = 1$ acting at ζ_j. The minus sign in the equation is due to the assumed opposite positive direction of P_i and w_i. In order to

evaluate the localized compliances, we consider an energy balance according to the formulation briefly recalled in Appendix A.

The kinematic conditions may be deduced from the physical action exerted by the reinforcements that bridge the crack, keeping it closed at their levels during the elastic phase and controlling its opening after yielding or slippage (Fig. 2(b, c)). Hence, a compatible solution sets the crack opening displacements w_i, $i = 1, \ldots, m$, equal to zero until yielding or slippage of at least one of the m reinforcements is reached (Fig. 2(b)). Using a matrix formulation, this condition takes on the form:

$$\{w\} = \{\lambda_M\}M - [\lambda]\{P\} = \{0\} \tag{7}$$

where $\{w\} = \{w_1, \ldots, w_m\}^T$ is the vector whose components are the crack opening displacements at the different fiber levels, $\{P\} = \{P_1, \ldots, P_m\}^T$ is the vector of the unknown fiber bridging reactions, $\{\lambda_M\}$ and $[\lambda]$ are respectively the vector $\{\lambda_{1M}, \ldots, \lambda_{mM}\}^T$ of the localized compliances related to the moment M and the symmetrical $m \times m$ matrix, whose generic element ij represents the localized compliance λ_{ij}. Resolution of the system leads to the unknown vector $\{P\}$ as a function of the applied moment:

$$\frac{\{P\}h}{M} = [\lambda]^{-1}\{\lambda_M\}h. \tag{8}$$

If the generic ith reinforcement yields or slips, the crack opens at the coordinate c_i, and w_i becomes an unknown quantity. The number of equations in system (7) reduces, as well as the degree of redundancy, P_i being equal to the previously defined maximum bridging force P_{Pi} (Fig. 2(c)). Also at the subsequent plastic deformations of the reinforcements, the number of the unknown quantities is again equal to the number of equations. By means of eqn (8) or the similar relationships for one or more reinforcements already yielded, the dimensionless plastic moment $M_{Pi}/(P_{Pi}h)$, for which the generic ith reinforcement reaches the yielding limit, can be evaluated. This depends on the crack length and the fiber positions only.

The moment of crack-propagation, M_F, corresponding to the crack in a state of mobile equilibrium, is evaluated through the superposition principle and the mobile equilibrium condition:

$$K_I = K_{IM} - \sum_{j=1}^{m} K_{Ij} = K_{IC} \tag{9}$$

in which K_I is the global crack tip stress intensity factor, and K_{IM} and K_{Ij} are the stress intensity factors due to the applied bending moment and to the generic opening forces P_j, respectively (see Appendix B). The dimensionless form of the crack-propagation moment is given by

$$\frac{M_F}{K_{IC}h^{1.5}b} = \frac{1}{Y_M(\xi)}\left\{\frac{N_P}{\rho}\sum_{i=1}^{m}\rho_i\frac{P_i}{P_{Pi}}Y_P(\xi, \zeta_i) + 1\right\} \tag{10}$$

in which N_P is the dimensionless number given in eqn (4). Relation (10) can be worked out by observing that the ratio P_i/P_{Pi} is equal to the ratio M_F/M_{Pi}, M_{Pi} being the previously evaluated plastic moment. Therefore, the applied moment for which a crack, whose length is fixed, reaches the onset of propagation, can be evaluated for the different conditions of the m reinforcements crossing the crack (yielded or unyielded). The cross-sectional resistance moment will be the minimum among these values.

The localized rotation due to the crack is a function of both the applied bending moment and the bridging reactions through the localized compliances:

$$\phi = \phi_M + \sum_{i=1}^{m} \phi_i = \lambda_{MM} M - \sum_{i=1}^{m} \lambda_{Mi} P_i = \lambda_{MM} M - \{\lambda_M\}^T \{P\} \tag{11}$$

in which ϕ_M and ϕ_i are the localized rotations due to M and to P_i, respectively, and λ_{MM} and λ_{Mi} are given by eqns (A11) and (A9). The dimensionless form of the localized rotation for the crack at the onset of propagation is

$$\phi = \frac{2K_{IC}}{Eh^{0.5}} \left\{ \frac{M_F}{K_{IC} h^{1.5} b} \int_0^{\xi} Y_M^2(\xi)\, d\xi - \frac{N_P}{\rho} \sum_{i=1}^{m} \frac{P_i}{P_{Pi}} \rho_i \int_{\zeta_i}^{\xi} Y_M(\xi) Y_P(\xi, \zeta_i)\, d\xi \right\} \tag{12}$$

where $K_{IC}/(Eh^{0.5})$ is the reciprocal of the dimensionless Young's modulus $\tilde{E}$.

Note that the particular dimensionless form of eqns (10) and (12) results from the dimensional analysis proposed in the previous section. Apart from a multiplicative constant quantity due to the geometrical ratio b/h, the left-hand side of eqn (10) represents, in fact, the dimensionless moment $\tilde{M}$ of the functional relationship (3). The dimensionless ultimate stress of the reinforcements appears in the equations through the dimensionless number N_P, and the dimensionless Young's modulus $\tilde{E}$ is present in eqn (12) as a divisory constant of the localized rotations. Equations (10) and (12) make it possible to verify that, if the beam geometrical ratios are fixed and the single reinforcements have the same percentage area, the cross-sectional flexural response is controlled by the dimensionless number N_P alone.

4. CROSS SECTION WITH TWO REINFORCEMENTS

The previously proposed theoretical formulation can be readily illustrated in the simple case of a beam with two layers of reinforcement, and this example brings out the essential nonlinear phenomena affecting the post-cracking behavior of any brittle-matrix composite member. Consider the composite beam shown in Fig. 2(a), in which only two equal reinforcements are placed at the normalized coordinates $\zeta_1 = c_1/h = 0.1$ and $\zeta_2 = c_2/h = 0.2$.

In the diagram of Fig. 4, the dimensionless crack-propagation moment $M_F/(K_{IC}h^{1.5}b)$ vs the normalized crack depth ξ relationship, is depicted. The thick curve represents the cross-sectional resistant moment when the reinforcements are still elastic, while the thin curves refer to one or both of the reinforcements when they have already yielded or slid, as varying the brittleness number N_P. The dots in the figure indicate the reinforcement yielding points.

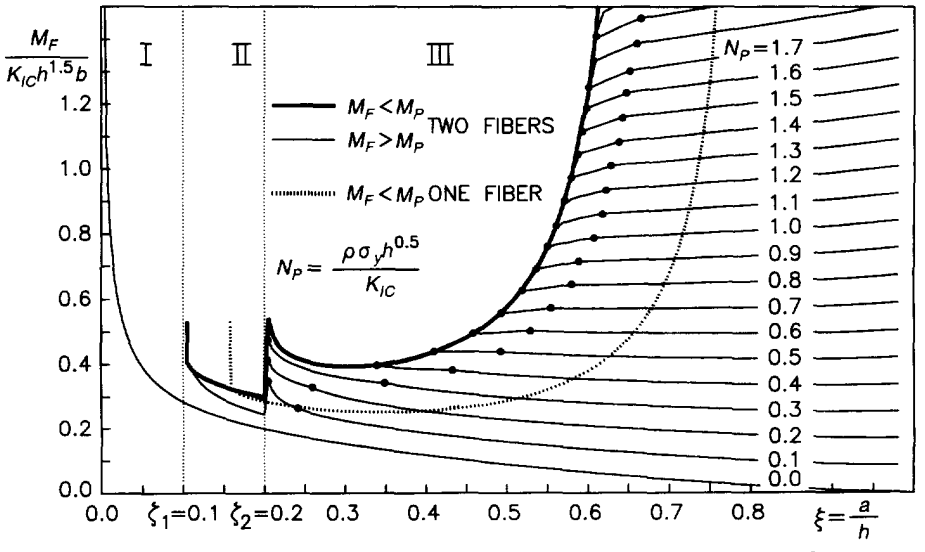

Fig. 4. Dimensionless crack-propagation moment vs normalized crack depth diagram for a composite cross section with one or two localized reinforcements.

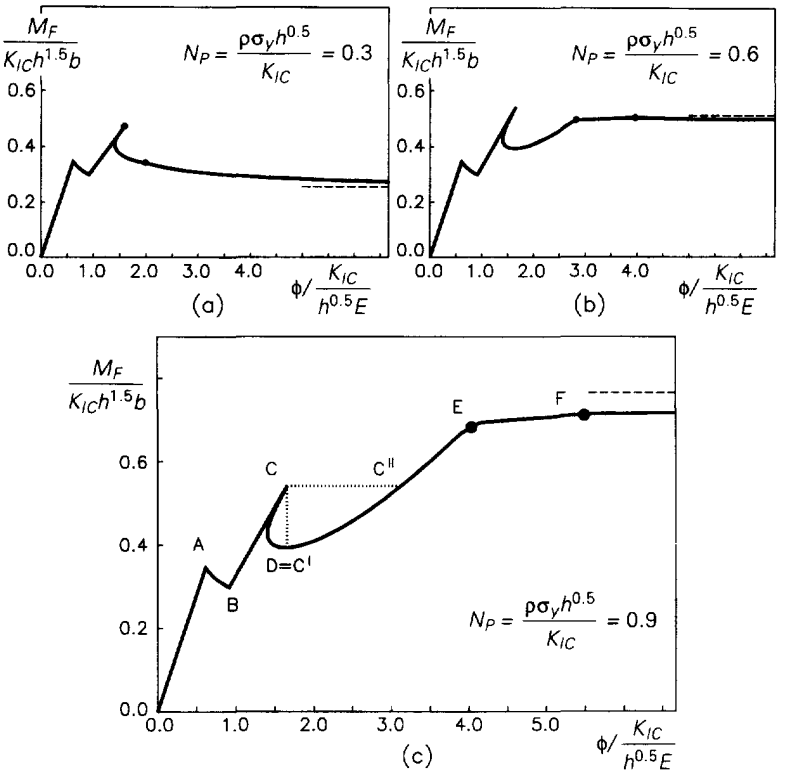

Fig. 5. Dimensionless moment vs localized rotation diagrams for a beam with two reinforcements, as the brittleness number N_P varies.

The diagram makes it possible to follow the evolutive process of crack propagation along the beam depth and is subdivided into three zones. Zone I, for $0 < \xi < \zeta_1$, concerns cracks in the plain matrix of the cross section cover, whose strain-softening response is controlled by the matrix toughness K_{IC} only and is represented by the curve for $N_P = 0$, i.e., $\rho = 0$. This curve characterizes the flexural response of a perfectly brittle material, which is stable only if a fast and uncontrollable crack propagation is avoided by a progressive decrease of the applied moment. Zone II, for $\zeta_1 < \xi < \zeta_2$, concerns crack depths between the reinforcements, and Zone III, for $\xi > \zeta_2$, cracks which have passed the innermost reinforcement. In these zones the reinforcements increase the toughness of the cross section, and the global response becomes more stable when the fiber percentage, and thus the brittleness number N_P, increases from zero ($N_P = 0$) to a greater value ($N_P > 0$). At the boundaries between the three zones, for crack depths equal to the fiber coordinates, the theoretical model predicts local discontinuities, with positive jumps of the resistance moment: when a propagating crack reaches a reinforcement it is arrested, and the new advancement takes place in response to an increment of the applied moment.

The dimensionless moment versus localized rotation relationships have been evaluated for three different sections, with brittleness numbers N_P of 0.3, 0.6 and 0.9, respectively, and with a normalized initial crack depth $\xi_0 = a_0/h = 0.12$. The curves are shown in Fig. 5, where the localized rotation in the abscissa is multiplied by the dimensionless parameter $\tilde{E}$. The diagrams refer to the initial part of the constitutive curves. The horizontal dashed lines represent the dimensionless ultimate moment for totally disconnected sections. These are asymptotes for the theoretical curves and, with the assumption of yielded reinforcements ($P_1 = P_2 = P_P$) at final collapse, are given by

$$\frac{M_u}{K_{IC}h^{1.5}b} = N_P\left(1 - \frac{\zeta_1 + \zeta_2}{2}\right). \tag{13}$$

A ductile-brittle transition clearly emerges in the diagrams of Fig. 5 when the brittleness

number N_P decreases. The first cross section, with $N_P = 0.3$, shows a global strain-softening response, whereas the last cross section, with $N_P = 0.9$, shows a global strain-hardening response. These results suggest that beams of different depth, but made with the same composite material, can show different structural responses (see eqn (4)). Moreover, the responses of different beams, with different heights, but with the same kind of matrix and reinforcements, can be similar if the product of the reinforcement percentage and the square root of the height is kept constant.

The theoretical results have been confirmed by several experimental tests carried out on different kinds of composite materials. The ductile-brittle transition has, for example, been reproduced by experimental tests on high-strength reinforced concrete by Bosco *et al.* (1990). Local discontinuities in some experimental flexural relationships have been shown in Fig. 1.

In order to trace the damage process occurring in the composite sections, consider the moment-vs-rotation curve of the beam with $N_P = 0.9$, shown in Fig. 5(c). The cross-sectional response is linear-elastic up to point A. In Fig. 4 this branch would be represented by a vertical path for $\xi = \xi_0$. An unstable crack propagation starts in A and goes on until in B the crack approaches the inner reinforcement and stops. The reinforcement bridging action increases the toughness of the cross section, and the applied moment value enabling a new crack propagation is suddenly increased. The new system condition is represented by point C, which is characterized by the same crack depth of point B (see Fig. 4). Note that the branch BC is linear. After reaching point C, the crack continues propagating in an unstable way until the local minimum D. Subsequently the cracking process is stable, and the applied moment must be progressively increased in order to produce the crack advancement. After point E, a marked reduction in stiffness and plastic deformations control the strain-hardening branch toward the asymptotic ultimate moment M_u. In F the inner reinforcement yielding is reached. The dotted lines $C-C'$ and $C-C''$ in Fig. 5(c), define a snap-back and a snap-through instability, respectively. The snap-back instability, or a jump at constant rotation, would be experimentally or theoretically obtained in a displacement-controlled process, while the snap-through instability, or a jump at constant load, would be obtained in a load-controlled process.

The number of reinforcements has been assumed fixed in the previous application, although it can affect the structural response of the composite section in bending. Consider a beam with a single layer of reinforcement, and assume the reinforcement coordinate equal to $c = 0.15h$, so that its lever arm with respect to the extrados equalizes that of the previously analyzed beam.

The nondimensional moment vs crack depth relationship is depicted in Fig. 4 through the dotted thick line (for elastic reinforcement) and through the thin lines (for yielded reinforcement). Note that the relationships for the two beams coincide after yielding of the reinforcements (thin lines).

In Fig. 6 the comparison between the moment-rotation curves, corresponding to the first beam (thin lines) and the second beam (thick lines), is shown. Two different brittleness numbers, $N_P = 0.3$ and $N_P = 0.6$, have been considered and an initial crack has been

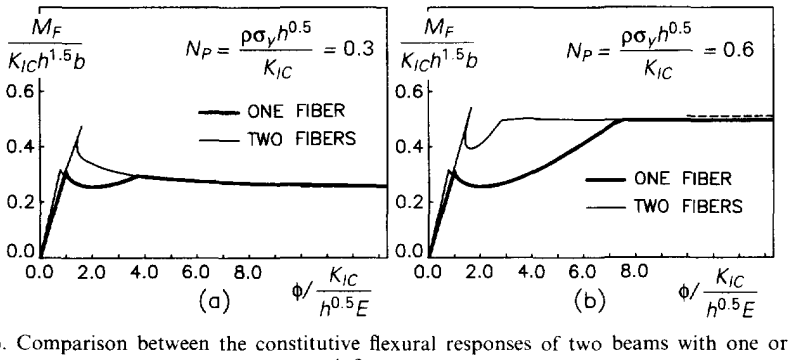

Fig. 6. Comparison between the constitutive flexural responses of two beams with one or two reinforcements.

assumed of depth $a_0 = 0.17h$. The different reinforcement distribution strongly affects the structural performance of the beam in the initial cracking phase, as the crack-propagation moment of the beam with two reinforcements proves greater than the corresponding moment of the beam with a single reinforcement (thick curve in Fig. 4). On the other hand, the reinforcement distribution does not modify the ultimate loads, which are controlled by the reinforcement lever arms and by the brittleness number through eqn (13), as well as the responses for very deep cracks (thin curves in Fig. 4). The curves relating to the beam with two reinforcements show a decrement of the system compliance and a less marked pop-in behavior.

The kinematic condition (7) provides an explanation for these results. In the beam with two reinforcements, the crack is kept closed in two points along the depth ($w_i = 0$, $i = 1, 2$), because of the reinforcement bridging action, up to reinforcement yielding or debonding. In this way the maximum amplitude of the eyelet, which describes the crack face shape, does not reach the amplitude developed in the singly-reinforced beam, given equal crack depth.

The above-mentioned considerations are fundamental in structural components whose cracking process and durability must be controlled. The same conclusions may be drawn when the number of the reinforcements is increased, and therefore the post-cracking structural behavior improves if the reinforcements are smeared in the cross section (provided the lever arm of the resultant bridging force and the brittleness number of the cross section N_P are kept unchanged). These theoretical results have been widely confirmed by experimental tests. Among others we may refer to the tests carried out by Nervi (1951), in which the above-mentioned phenomena were observed in the flexural response of cementitious members reinforced with smeared steel wires.

5. CONTINUOUS MODEL

The continuous model has been formulated for the macrostructural analysis of multiphase composites, consisting of brittle matrices and continuously distributed secondary phases. The model derives from the discontinuous model with the assumption of rendering homogeneous the secondary-phase bridging action (Fig. 3).

As in the previously proposed discontinuous model, a loading process, controlled by the crack advancement, is theoretically simulated in order to predict the constitutive flexural behavior of the cross section. The analytic formulation has been developed by Carpinteri and Massabó (1995), for a generic bridging relationship $\sigma_0(w)$, to describe different secondary phases. This requires the resolution of a nonlinear integral problem which involves the verification of both kinematic compatibility and static equilibrium. Nevertheless, when the bridging relationship can be described by a rigid-plastic law, as for the continuous ductile reinforcements of the composite material under consideration, the problem can be simply solved by checking the equilibrium conditions.

Consider the cracked beam in bending shown in Fig. 3. The total crack of depth a is given by the addition of two portions, the real or traction-free crack of depth a_r, along which the crack faces have no interaction, and the bridged crack of depth $(a - a_r)$, acted upon by the bridging tractions $\sigma_0(w)$.

A singular stress field is assumed in the crack tip vicinity and the total crack tip stress intensity factor K_I is defined, through the superposition principle, as the sum of the stress intensity factors K_{IM}, eqn (B1), and $K_{I\sigma}$, respectively, due to the bending moment M and to the closing tractions σ_0. The factor $K_{I\sigma}$ is obtained by integrating along the bridged crack the product between the stress intensity factor due to opposite opening forces $P_j = 1$ applied at the generic coordinate ζ_j (eqn (B3)) and the bridging tractions σ_0, thus:

$$K_{I\sigma} = \int_{\xi r}^{\xi} \frac{K_{Ij}(\xi, \zeta_j)}{P_j} \sigma_0(w(\zeta_j)) bh \, d\zeta_j = \frac{1}{h^{0.5} b} \int_{\xi r}^{\xi} \sigma_0(w(\zeta)) \, Y_P(\xi, \zeta) bh \, d\zeta. \tag{14}$$

The crack propagates when K_I equalizes the matrix toughness K_{IC}.

$$\frac{M}{h^{1.5}b}Y_M(\xi)-\frac{1}{h^{0.5}b}\int_{\xi r}^{\xi}\sigma_0(w(\zeta))\,Y_P(\xi,\zeta)bh\,\mathrm{d}\zeta=K_{IC}. \tag{15}$$

Relationships (4) and (15) yield the dimensionless moment of crack propagation

$$\frac{M_F}{K_{IC}h^{1.5}b}=\frac{1}{Y_M(\xi)}\left\{N_P\int_{\xi r}^{\xi}\frac{\sigma_0(w(\zeta))}{\rho\sigma_y}Y_P(\xi,\zeta)\,\mathrm{d}\zeta+1\right\}. \tag{16}$$

At the onset of propagation, the bridging tractions $\sigma_0(w)$ have reached the ultimate value $\rho\sigma_y$, and therefore eqn (16) simplifies as follows:

$$\frac{M_F}{K_{IC}h^{1.5}b}=\frac{1}{Y_M(\xi)}\left\{N_P\int_{\xi r}^{\xi}Y_P(\xi,\zeta)\,\mathrm{d}\zeta+1\right\}. \tag{17}$$

The localized rotation ϕ of the cracked cross section takes the form:

$$\phi=\phi_M+\phi_\sigma=\lambda_{MM}(\xi)M-\int_{\xi r}^{\xi}\lambda_{Mj}(\xi,\zeta_j)\sigma_0(w(\zeta_j))bh\,\mathrm{d}\zeta_j \tag{18}$$

where ϕ_M and ϕ_σ are the rotations due to the applied bending moment and to the closing tractions, respectively, and λ_{MM} and λ_{Mj} are the localized compliances due to the crack, given by eqns (A11) and (A9). By substituting eqn (17) into eqn (18), the localized rotation at the onset of crack propagation turns out to be

$$\phi=\frac{2K_{IC}}{Eh^{0.5}}\left\{\frac{M_F}{K_{IC}h^{1.5}b}\int_0^{\xi}Y_M^2(y)\,\mathrm{d}y-N_P\int_{\xi r}^{\xi}\left(\int_{\zeta}^{\xi}Y_M(y)\,Y_P(y,\zeta)\,\mathrm{d}y\right)\mathrm{d}\zeta\right\}. \tag{19}$$

In Fig. 7 the theoretical curves relating the dimensionless crack-propagation moment

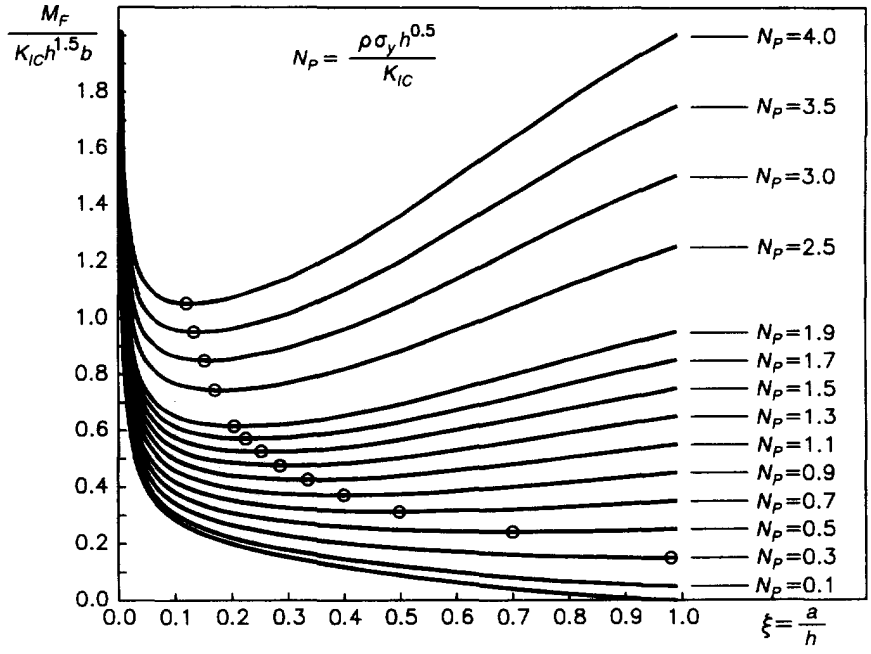

Fig. 7. Dimensionless crack-propagation moment vs normalized crack depth diagram for a composite cross section with uniformly distributed ductile reinforcements.

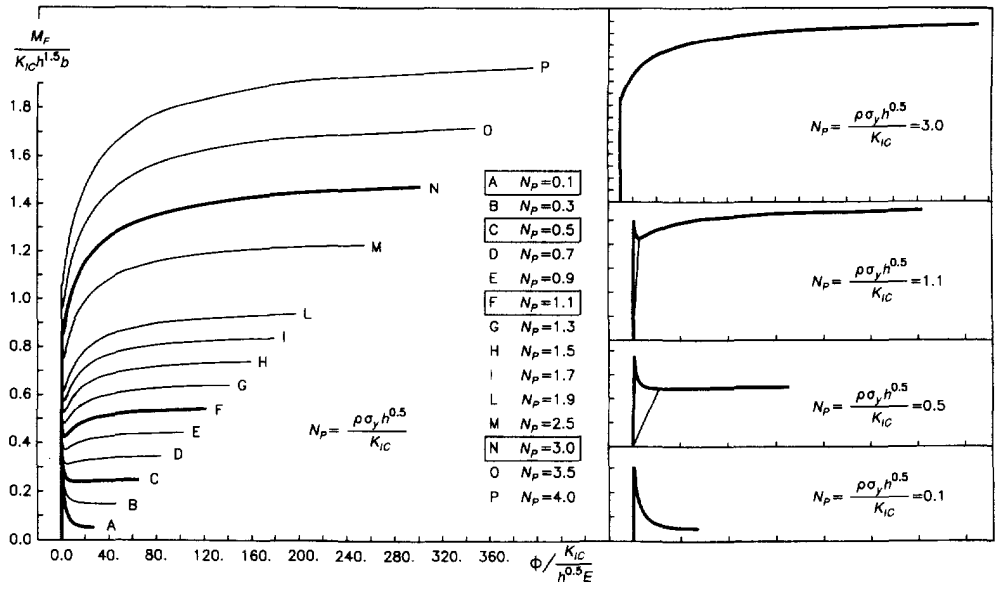

Fig. 8. Dimensionless moment vs localized rotation diagrams for a continuously reinforced beam as the brittleness number N_P varies.

$M_F/(K_{IC}h^{1.5}b)$ to the normalized crack depth ξ are shown for a beam whose reinforcements are smeared in the whole cross section, as the brittleness number N_P varies. According to LEFM, the crack-propagation moment tends to be infinite when the crack depth vanishes. The circles in the figure indicate the minimum of each curve, which represents a transition in the evolutive process of crack propagation. For crack depths lower than that corresponding to the minimum, the response is unstable and an uncontrollable crack propagation can be avoided only by progressively decreasing the applied load. On the other hand, for crack depths greater then the limit value, the process is stable, and a slow crack growth is made possible only by increasing the applied load. The limit crack depth increases when the brittleness number decreases, and for N_P lower than 0.1, the crack propagation process is always unstable.

The corresponding moment versus localized rotation diagram is shown in Fig. 8. The theoretical curves have been obtained by assuming an initial matrix crack of depth $a_0 = 0.1h$, bridged by unbroken reinforcements ($\xi_r = 0$). The curves tend asymptotically to the ultimate dimensionless moment for totally disconnected sections

$$\frac{M_u}{K_{IC}h^{1.5}b} = N_P\frac{(1-\xi_r)^2}{2} = \frac{N_P}{2} \tag{20}$$

Some constitutive curves, for $N_P = 0.1$, 0.5, 1.1 and 3.0 are drawn again in the small diagrams given alongside. A ductile to brittle transition emerges as N_P decreases, i.e. as the beam depth or the fiber volume ratio decreases, or the matrix toughness increases. This behavior has been experimentally verified in fiber reinforced concrete beams by Gopalaratnam *et al.* (1995).

The curves with $N_P = 1.1$ and $N_P = 0.5$ show a hyper-strength phenomenon, the maximum load bearable by the beams being greater than the ultimate load at the total disconnection. In fact, for low brittleness numbers the matrix toughness, which controls the first post-cracking response, prevails over the toughening mechanism due to the secondary phases, which instead controls the response for deep cracks. This phenomen has been experimentally noticed in the flexural response of reinforced concrete beams by Bosco *et al.* (1990) and by Levi *et al.* (1988), and it is usually detected in the flexural response of fiber-reinforced cementitious materials (Jenq and Shah, 1986).

Local snap-through instabilities can be observed in the theoretical curves characterized by intermediate values of N_P, which tend to disappear when the brittleness number increases

as the toughening mechanism of the secondary phases starts to prevail over the toughening mechanism of the brittle matrix. At the limit, for a very high N_P number, the flexural response could be consistently reproduced by means of a theoretical model disregarding the matrix toughness ($K_{IC} = 0$).

The depth of the assumed initial crack affects the mechanical responses. The thin lines in the small diagrams of Fig. 8, for $N_P = 0.5$ and $N_P = 1.1$, represent the linear elastic behavior of beams whose initial crack has been assumed equal to the limit value defined by the circle in Fig. 7, $a_0 \simeq 0.7h$ and $a_0 \simeq 0.33h$ for $N_P = 0.5$ and $N_P = 1.1$, respectively. The post-cracking responses of these two cases are defined by the same curves previously obtained for an initial crack depth of $0.1h$, and therefore the beam with $N_P = 0.5$ shows an elastic-plastic behavior, while the beam with $N_P = 1.1$ presents a strain-hardening response.

The above results emerge from the assumption of a perfectly plastic bridging relationship. On the other hand, different responses would be predicted if the rigid-plastic bridging tractions $\sigma_0(w)$ vanished for a critical value of the crack opening displacement w_c. The constitutive flexural response of this material would be depicted by eqns (16) and (19), which continue to be applicable, provided the length of the fully bridged crack $(\xi - \xi_r)$, along which the integrals are evaluated, corresponds to the equilibrated and compatible solution.

Without entering into the details of this new problem, which has been studied by Carpinteri and Massabó (1995), it is interesting to report for completeness some conclusions. Figure 8 has pointed out the existence of a size-scale effect, represented by a brittle-ductile transition in the constitutive flexural response, as the beam characteristic dimension h increases, while the mechanical properties are kept unchanged. On the other hand, if the traction-free crack propagates during the loading process, the structural component can verify a size-scale effect characteristic of the strain-softening material, which is opposite to the preceding one and represented by a ductile-brittle transition.

6. CONTINUOUS VS DISCONTINUOUS STRUCTURAL RESPONSES

The constitutive response of composites with a limited number of localized reinforcements, or the influence of the single reinforcements on the crack extension can be investigated by means of the proposed discontinuous model. On the other hand, the continuous model can be consistently applied to make macrostructural studies of multiphase nonlinear materials. Nevertheless, if the number of the individual reinforcements in the member is high enough, the discontinuous and the continuous model converge to the same global results.

In order to make a comparison between the theoretical results, a beam reinforced with ten continuous fibers, equally distributed in the part of the cross section between $0.1h$ and $0.55h$, has been considered. The beam is initially notched and $a_0 = 0.1h$. Three different situations, for brittleness numbers N_P of 0.1, 0.4 and 0.7, respectively, have been considered.

The structural behavior has been studied using the previously proposed discontinuous (Bosco and Carpinteri, 1991) and continuous models. In order to apply the continuous model, a uniform equivalent distribution of reinforcements has been applied along the crack faces in place of the localized fibers. The two schemes are shown in Fig. 9(a). In the same figure, the theoretical diagrams relating the dimensionless crack-propagation moment $M_F/(K_{IC}h^{1.5}b)$ to the normalized rotation ϕ/ϕ_0 are depicted. The localized rotation ϕ has been normalized with respect to the rotation ϕ_0 at the propagation of the initial crack. The thick lines and the thin lines represent the flexural responses predicted by the discontinuous model and the continuous model, respectively. The horizontal dashed lines define the ultimate moment of the cross section.

A substantial agreement is noticeable in the global responses. Both the models predict the already observed brittle to ductile transition for increasing N_P.

The thick curves, resulting from the discontinuous model, show a discontinuous initial branch, presenting the characteristic saw-tooth appearance which reveals local instabilities. This part of the curve describes the cross-sectional behavior during crack advancement until the last fiber position $c_{10} = 0.55h$ is reached. The repeated crack initiation and arrest,

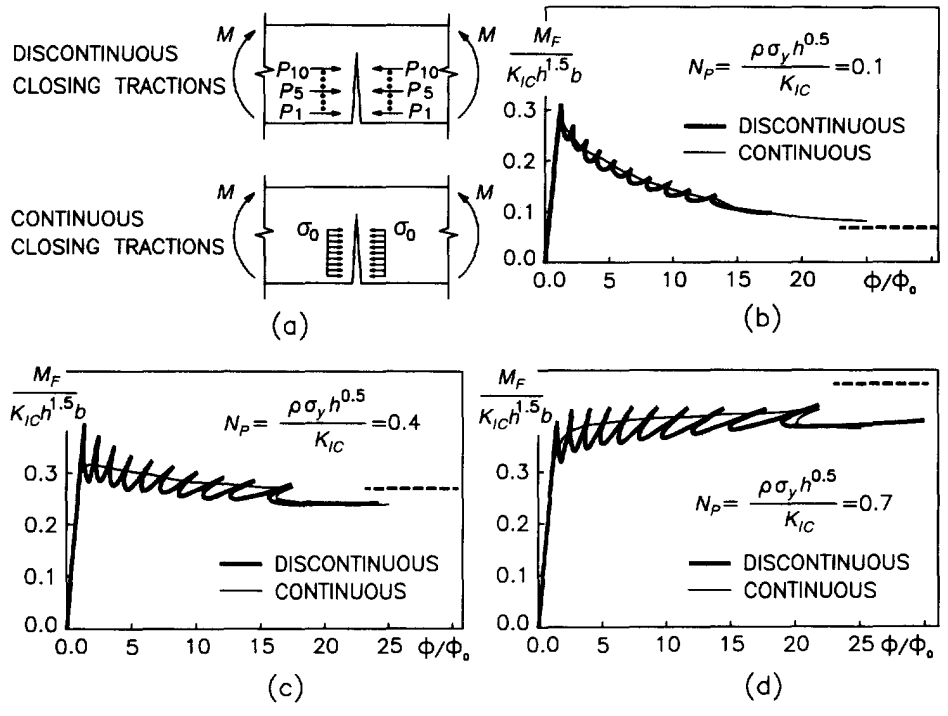

Fig. 9. Comparison between the discontinuous and the continuous theoretical results: (a) theoretical schemes; (b), (c) and (d) dimensionless moment vs localized rotation diagrams.

due to the bridging action of the individual fibers, give rise to this pattern. The saw-tooth maxima are the points at which the crack growth initiates, while the saw-tooth minima are the points of crack arrest. This kind of discontinuous response is very evident in brittle matrices reinforced with high-strength and high-bond resistance continuous or discontinuous fibers (see Fig. 1). Often the same phenomenon appears in the response of other kinds of composite materials, but usually it is less pronounced owing to the matrix nonlinear behavior and to the sliding and pull-out mechanisms of the reinforcements that smooth the saw-tooth peaks (Bosco *et al.*, 1990).

The thin curves, resulting from the continuous model, define a continuous response which averages the discontinuous one. The localized rotations predicted by the two models are the same as demonstrated by the snap-back in the thin curves, appearing as soon as the crack penetrates the unbridged matrix, the position of which coincides with the last discontinuity of the thick discontinuous curve.

The results of this section can be explained by comparing eqns (10) and (12) with eqns (17) and (19), of the discontinuous and the continuous model, respectively. The integrals in eqns (17) and (19), in place of the summations in eqns (10) and (12), are explained by the assumed homogenization of the localized fibers. Moreover, the discontinuous model assumes that the fibers crossing the crack can be still elastic when the crack is about to propagate, ($P_i < P_{Pi}$ or $\sigma_i < \sigma_y$) and it evaluates the bridging reactions through the kinematic condition (7) according to which the crack remains closed until the plastic deformation of the reinforcement is reached. This assumption does not prevent the crack face opening between the single fibers and therefore the growth of localized rotations (Fig. 2(b)). On the other hand, the continuous model assumes that the bridging tractions have already reached the yielding limit at the onset of crack propagation, without making any distinction between the potential collapse of crack propagation and reinforcement yielding, which occur at the same time.

The comparison in Fig. 9 shows that the increase in the fiber number, and therefore the reduction in the fiber spacing, tends to produce a real monophase behavior. In these terms the structural response could be modelled not only by a continuous bridged-crack model, but also by a cohesive-crack model, according to which the toughening mechanism

of both the matrix and the secondary elements are combined and a single cohesive relationship $\sigma_0(w)$ for the whole composite is defined (Carpinteri and Massabó, 1995).

It is worth specifying that when the reinforcement number is low, e.g. the two fibers of the example in Fig. 5, the application of the continuous model, by smearing the bridging tractions over a zone surrounding the position of the reinforcements, would lead to totally erroneous results in the loading phase preceding the yielding of the reinforcements. This is due to the continuous model assumption of yielded reinforcements at the onset of crack propagation.

7. CONCLUSIONS

Two nonlinear fracture mechanics models have been proposed for the analysis of the failure process in brittle-matrix composite materials, which consider the two competing potential crises of brittle crack propagation and reinforcement yielding or debonding. The *discontinuous model* is a bridged-crack model for the analysis of composite beams in bending with a limited number of localized reinforcements. The same model can be applied to microscale analysis of brittle matrix composites with continuously distributed secondary phases when the localized action of the single reinforcements on the discontinuous crack-propagation process is of interest. The model reproduces local discontinuities in the moment vs rotation constitutive response caused by the reinforcement bridging action. The *continuous model* has been derived from the discontinuous model with the assumption of rendering homogeneous the secondary-phase action. It can be consistently applied to macrostructural analysis of multiphase materials with a continuous distribution of reinforcements.

The mechanical behavior proves to be governed by one or two dimensionless parameters according to the assumed bridging law, which describes the secondary-phase resistance against crack opening and propagation. For a rigid-perfectly plastic law, representative of the bridging mechanism of long ductile fibers, the single parameter is the dimensionless number $N_P = \rho\sigma_y h^{0.5}/K_{IC}$. For a rigid-plastic law limited by a critical value of the crack opening displacement, a second dimensionless parameter $\tilde{E}\tilde{w} = Ew_c/(K_{IC}h^{0.5})$ may affect the structural response. Physical similitude in the structural responses is predicted if the dimensionless parameters are kept unchanged.

For a composite material whose bridging mechanism may be represented by a perfectly plastic law, both the proposed models predict a ductile-brittle transition in the failure when the brittleness number N_P decreases. This means that a size-scale effect is predicted in the composite constitutive response according to which it modifies from strain-softening to strain-hardening when the beam depth increases. Nevertheless, this trend may undergo modification, if a critical crack opening displacement exists beyond which the bridging tractions vanish.

In a composite with a sufficiently high number of localized reinforcements, the two theoretical models converge to the same global results. The continuous model, albeit without reproducing the local discontinuities and the characteristic saw-tooth behavior in the constitutive flexural response of the cross section, nevertheless defines an average behavior. At the limit, the increase in the fiber number, and therefore the reduction in the fiber spacing, tends to produce in the composite material a real monophasic behavior and this could be modeled as homogeneous.

Acknowledgements—The authors gratefully acknowledge the financial support of the National Research Council (CNR) and the Department for the University and for Scientific and Technological Research (MURST).

REFERENCES

Ballarini, R. and Muju, S. (1993) Stability analysis of bridged cracks in brittle matrix composites. *Journal of Engineering Gas Turbines Power* **115**, 127–138.

Bosco, C., Carpinteri, A. and Debernardi, P. G. (1990) Minimum reinforcement in high-strength concrete. *Journal of Structural Engineering* **116**, 427–437.

Bosco, C. and Carpinteri, A. (1991) Fibre toughening and crack growth stability in fiber-reinforced disordered materials. *Proc. of the Int. Conf. on Fracture in Brittle Disordered Materials*, Noordwijk, The Netherlands, Vol. 1, 295–305.

Bosco, C. and Carpinteri, A. (1992a) Softening and snap-through behavior of reinforced elements. *Journal of Engineering and Mechanics* **118,** 1564–1577.

Bosco, C. and Carpinteri, A. (1992b) Fracture behavior of beam cracked across reinforcement. *Theoretical and Applied Fracture Mechanics* **17,** 61–68.

Bosco, C. and Carpinteri, A. (1995) Discontinuous constitutive response of brittle matrix fibrous composites. *Journal of Mechanics, Physics and Solids* **43,** 261–274.

Buckingham, E. (1915) Model experiments and the form of empirical equations. *Transactions of ASME* **37,** 263–296.

Budiansky, B., Hutchinson, J. W. and Evans, A. G. (1986) Matrix fracture in fiber-reinforced ceramics. *Journal of Mechanics, Physics and Solids* **34,** 167–189.

Carpinteri, A. (1981). A fracture mechanics model for reinforced concrete collapse. *Proc. of the IABSE Colloquium on Advanced Mechanics of Reinforced Concrete*, Delft, The Netherlands, pp. 17–30.

Carpinteri, A. (1984) Stability of fracturing process in r.c. beams. *Journal of Structural Engineering* **110,** 544–558.

Carpinteri, A. and Massabó, R. (1994) Continuous versus discontinuous bridged crack in the description of reinforced material flexural collapse. *Proc. of the Int. Conf. on Computational Modelling of Concrete Structures*, eds H. Mang, N. Bicanic and R. de Borst. Vol. 1, pp. 233–242. Pineridge Press Limited, Swansea, U.K.

Carpinteri, A. and Massabó, R. (1995) Nonlinear fracture mechanics models for fibre reinforced materials. *Proc. Int. Symposium on Advanced Technology for Design and Fabrication of Composite Materials and Structures* (1993) eds G. C. Sih, A. Carpinteri and G. Surace, pp. 31–48. Kluwer Academic Publishers, Dordrecht, The Netherlands.

Cox, B. N. and Marshall, D. B. (1991) Stable and unstable solutions for bridged cracks in various specimens. *Acta Metallurgical Materials* **39,** 579–589.

Cox, B. N. (1991) Extrinsic factors in the mechanics of bridged cracks. *Acta Metallurgical Materials* **39,** 1189–1201.

Cox, B. N. and Marshall, D. B. (1994) Concepts for bridged cracks in fracture and fatigue. *Acta Metallurgical Materials* **42,** 341–363.

Desayi, P. and Ganesan, N. (1986) Fracture behavior of ferrocement beams. *Journal of Structural Engineering* **112,** 1509–1525.

Erdogan, F. and Joseph, P. F. (1989) Toughening of ceramics through crack bridging by ductile particles. *Journal of the American Ceramic Society* **72,** 262–270.

Foote, R. M. L., Mai, Y. W. and Cotterell B. (1986) Crack growth resistance curves in strain-softening materials, *Journal of Mechanics, Physics and Solids* **34,** 593–607.

Gopalaratnam, V. S., Gettu, R., Carmona, S. and Jamet D. (1995) Characterization of the toughness of fiber reinforced concretes using the load-cmod response. In *Fracture Mechanics of Concrete Structures*, Proc. FRAMCOS-2, ed. F. H. Wittman. pp. 769–782. Aedificatio, Freiburg.

Jenkins, M. G., Kobayashi, A. S., White, K. W. and Bradt, R. C. (1987) Crack initiation and arrest in a SiC whisker/Al_2O_3 matrix composite. *Journal of the American Ceramic Society* **70,** 393–395.

Jenq, Y. S. and Shah, S. P. (1985) Two parameter fracture model for concrete. *Journal of Engineering Mechanics* **111,** 1227–1241.

Jenq, Y. S. and Shah, S. P. (1986) Crack propagation in fiber-reinforced concrete. *Journal of Engineering Mechanics* **112**(1), 19–34.

Kendall, K., Clegg, W. J. and Gregory, R. D. (1991) Growth of tied cracks: a model for polymer crazing. *Journal of Material Science Letters* **10,** 671–674.

Levi, F., Bosco, C. and Debernardi, P. G. (1988) Two aspects of the behavior of slightly reinforced structures. *CEB Bulletin d'Information* **185,** 39–50.

Marshall, D. B., Cox, B. N. and Evans, A. G. (1985) The mechanics of matrix cracking in brittle-matrix fiber composites. *Acta Metallurgical Materials* **33,** 2013–2021.

Nervi, P. L. (1951) Il ferro-cemento: sue caratteristiche e possibilitá. *L'Ingegnere* **1,** 17–25.

Romualdi, J. P. and Batson, G. B. (1963) Behavior of reinforced concrete beams with closely spaced reinforcement. *Journal of ACI* **60–40,** 775–789.

Rose, L. R. F. (1987) Crack reinforcement by distributed springs. *Journal of Mechanics, Physics and Solids* **35,** 383–405.

Swanson, P. L., Fairbanks, C. J., Lawn, B. R., Mai, Y. W. and Hockey, B. J. (1987) Crack interface grain bridging as a fracture resistance mechanism in ceramics: II. theoretical fracture mechanics model. *Journal of the American Ceramic Society* **70,** 289–294.

Tada, H., Paris, P. C. and Irwin, G. (1985) *The Stress Analysis of Cracks Handbook*. Paris Productions Incorporated (and Del Research Corporation), St. Louis, Missouri.

Zhu, W. and Bartos, P. J. M. (1993) Effects of combined fiber treatments and matrix modifications on toughness of aged GRC. *Proc. of the 9th Congress of the GRCA*, Copenhagen, Denmark, 4/I–IX.

APPENDIX A

Consider the linear-elastic specimen shown in Fig. A1, which is subjected to n generalized concentrated forces P_i, $i = 1, \ldots, n$. The element of thickness b has a through-thickness crack of depth a. The generic load-point displacement δ_{iT} is given by the sum of the displacement δ_{i0} of the uncracked specimen plus the localized displacement δ_i due to the crack. The localized displacement δ_i is defined by the following equation:

$$\delta_i = \sum_{j=1}^{m} \lambda_{ij} P_j \tag{A1}$$

in which λ_{ij} are the localized compliances, namely the load-point displacement δ_i due to the unit load $P_j = 1$.

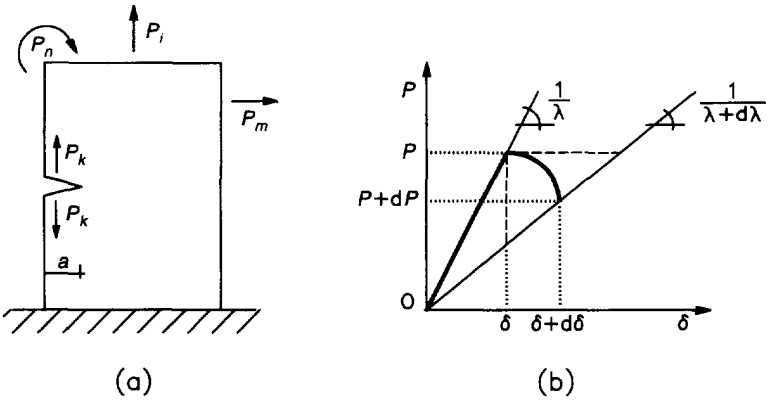

Fig. A1. Theoretical scheme for the evaluation of the localized compliances.

If the crack propagates by da the new specimen configuration will be characterized by new values of the loads and of the localized displacements, P_i+dP_i and $\delta_i+d\delta_i$ $(i=1,\ldots,n)$. The localized compliances will be incremented by $d\lambda_{ij}$. The variation of the total potential energy of the system consequent to the crack advancement is $dW=dU-dL$, dU and dL being the variations of the elastic strain energy and the potential of the applied loads, respectively. Applying Clapeyron's theorem, we obtain

$$dW=\sum_{i=1}^{n}\sum_{j=1}^{n}\left\{\frac{1}{2}P_j\,d\delta_i+\frac{1}{2}\delta_i\,dP_j-P_j\,d\delta_i\right\}. \tag{A2}$$

The meanings of the different terms on the right-hand side can be readily deduced from the load vs displacement diagram of Fig. A1(b) for the problem of a single applied load P. By expressing the increment of the localized displacement $d\delta_i$ as a function of the localized compliances

$$d\delta_i=\sum_{k=1}^{n}(\lambda_{ik}\,dP_k+P_k\,d\lambda_{ik}) \tag{A3}$$

and substituting eqn (A3) into eqn (A2), we obtain

$$dW=-\sum_{i=1}^{n}\sum_{j=1}^{n}\frac{1}{2}P_iP_j\,d\lambda_{ij}. \tag{A4}$$

The total potential energy W, the crack driving force $\mathcal{G}$ and the global crack tip stress intensity factor K_I are connected by the relation

$$dW=-\mathcal{G}b\,da=-\frac{(K_{I1}+\cdots+K_{In})^2}{E}b\,da=-\sum_{i=1}^{n}\sum_{j=1}^{n}\frac{(K_{Ii}K_{Ij})}{E}b\,da \tag{A5}$$

in which K_I is the sum of the stress intensity factors produced by all the applied loads. Integration of eqns (A4) and (A5) leads to two different expressions of the potential energy W:

$$W=-\int_0^a\mathcal{G}b\,da=-\sum_{i=1}^{n}\sum_{j=1}^{n}\int_0^a\frac{(K_{Ii}K_{Ij})}{E}b\,da \tag{A6}$$

$$W=-\sum_{i=1}^{n}\sum_{j=1}^{n}\frac{1}{2}P_iP_j\lambda_{ij} \tag{A7}$$

from which it is possible to define the generic localized compliances λ_{ij}:

$$\lambda_{ij}=\frac{2}{E}\int_0^a\frac{K_{Ii}K_{Ij}}{P_iP_j}b\,da. \tag{A8}$$

According to Betti's theorem, $\lambda_{ij}=\lambda_{ji}$.

For the beam in bending in Fig. 2(a) the localized compliances λ_{iM}, λ_{ij} and λ_{MM} in eqns (6) and (11) can be obtained by substituting the stress intensity factors of eqns (B1) and (B3)

$$\lambda_{iM} = \frac{2}{hbE}\int_{\zeta_i}^{\xi} Y_P(\xi,\zeta_i)\,Y_M(\xi)\,\mathrm{d}\xi \tag{A9}$$

$$\lambda_{ij} = \lambda_{ji} = \frac{2}{bE}\int_{\max[\zeta_i,\zeta_j]}^{\xi} Y_P(\xi,\zeta_i)\,Y_P(\xi,\zeta_j)\,\mathrm{d}\xi \tag{A10}$$

$$\lambda_{MM} = \frac{2}{Eh^2b}\int_0^{\xi} Y_M^2(\xi)\,\mathrm{d}\xi. \tag{A11}$$

Both the integrals in eqns (A9) and (A10) are improper since the integrand has a singularity in the interval of integration. The singularity in eqn (A9) is apparent and removable, while the one in eqn (A10), for $i = j$, is not removable and the integral diverges. To overcome this problem we can recall the initial assumption of the theoretical model concerning the substitution of the single reinforcement bridging action by means of two concentrated forces, so disregarding the transverse reinforcement dimension which is different from zero and known. If d is the diameter of the reinforcement and $\tilde{d} = d/h$ the normalized value, the ith fiber action on the crack could be represented by a closing traction distribution $p_i = P_i/bd$ acting between $c_i - d/2$ and $c_i + d/2$.

With this assumption, the local compliance λ_{ip_i}, representing the crack opening displacement at the fiber level c_i due to a unit traction distribution $p_i = 1$, can be defined by means of the following equation:

$$\lambda_{ip_i} = \frac{2}{Eb}\frac{1}{\tilde{d}}\int_{\zeta_i}^{\xi}\int_{\zeta_i-(\tilde{d}/2)}^{\min[y,\zeta_i+(\tilde{d}/2)]} Y_P(y,\zeta)\,\mathrm{d}\zeta\,Y_P(y,\zeta_i)\,\mathrm{d}y. \tag{A12}$$

The improper integral in the foregoing equation converges as the singularity can be removed. To represent in any case the fiber action by means of two concentrated forces, the local compliances in eqn (A10), for $i = j$, can be evaluated through

$$\lambda_{ii} = \frac{2}{Eb}\int_{\zeta_i+\frac{t}{h}}^{\xi} Y_P(\xi,\zeta_i)^2\,\mathrm{d}\xi \tag{A13}$$

where t/h is a proper normalized cut-off distance, calculated so that the local compliances λ_{ii}, eqn (A10), and λ_{ip_i}, eqn (A12), have the same numerical value ($t/h = 10^{-5}$).

APPENDIX B

$$K_{1M} = \frac{M}{h^{1.5}b}\,Y_M(\xi) \tag{B1}$$

$$Y_M(\xi) = \begin{cases} 6(1.99\xi^{0.5} - 2.47\xi^{1.5} + 12.97\xi^{2.5} - 23.17\xi^{3.5} + 24.8\xi^{4.5}), & \xi \leqslant 0.6 \\ \dfrac{3.99}{(1-\xi)^{1.5}}, & \xi \geqslant 0.6. \end{cases} \tag{B2}$$

$$K_{1j} = \frac{P_j}{h^{0.5}b}\,Y_P(\xi,\zeta_j) \tag{B3}$$

$$Y_P(\xi,\zeta_j) = \frac{2}{\sqrt{\pi\xi}}\frac{1}{(1-\xi)^{1.5}\sqrt{1-\left(\frac{\zeta_j}{\xi}\right)^2}}\,G(\xi,\zeta_j)$$

$$G(\xi,\zeta_j) = g_1(\xi) + g_2(\xi)\frac{\zeta_j}{\xi} + g_3(\xi)\left(\frac{\zeta_j}{\xi}\right)^2 + g_4(\xi)\left(\frac{\zeta_j}{\xi}\right)^3$$

$$g_1(\xi) = 0.46 + 3.06\xi + 0.84(1-\xi)^5 + 0.66\xi^2(1-\xi)^2$$

$$g_2(\xi) = -3.52\xi^2$$

$$g_3(\xi) = 6.17 - 28.22\xi + 34.54\xi^2 - 14.39\xi^3 - (1-\xi)^{1.5} - 5.88(1-\xi)^5 - 2.64\xi^2(1-\xi)^2$$

$$g_4(\xi) = -6.63 + 25.16\xi - 31.04\xi^2 + 14.41\xi^3 + 2(1-\xi)^{1.5} + 5.04(1-\xi)^5 + 1.98\xi^2(1-\xi)^2. \tag{B4}$$